Carbohydrate Polymers 114 (2014) 279–287

Contents lists available at ScienceDirect

Carbohydrate Polymers

journal homepage: www.elsevier.com/locate/carbpol

Rheology and pressurised gyration of starch and starch-loaded poly(ethylene oxide)

S. Mahalingam [a,*], G.G. Ren [b], M.J. Edirisinghe [a]

[a] Department of Mechanical Engineering, University College London, London WC1E 7JE, UK
[b] School of Engineering and Technology, University of Hertfordshire, Hatfield AL10 9AB, UK

ARTICLE INFO

Article history:
Received 12 November 2013
Received in revised form 4 July 2014
Accepted 4 August 2014
Available online 15 August 2014

Keywords:
Starch
Polymer
Nanofibres
Pressure
Gyration

ABSTRACT

This work investigates the rheology and spinning of starch and starch-loaded poly(ethylene oxide) (PEO) by pressurised gyration in order to prepare nanofibres. The spinning dope's rheological properties played a crucial role in fibre formation. Newtonian behaviour is observed in 1–20 wt% starch suspensions and non-Newtonian behaviour is found in all the PEO–starch mixtures. Pressurised gyration of the starch suspensions produced beads only but PEO–starch mixtures generated fibres. The fibre diameter of the PEO–starch samples is shown to be a function of polymer concentration and rotating speed of the gyration system. Fibre formation can only be facilitated below a certain working pressure. The concentration of starch in the PEO–starch mixtures is crucial in defining whether beaded or continuous fibres were generated and this is related to the composition of the spinning dope. FT-IR, XRD and microscopy studies indicated very good miscibility of starch and PEO in the nanofibres. The storage modulus of the PEO–starch were also studied as a function of temperature (30–150 °C) and showed interesting results but it was not possible to deduce general trends valid for the entire temperature range.

1. Introduction

Naturally occurring biopolymers have been used to produce nanofibres and nanofibrous structures with excellent functionality (Woodings, 2001). Of these, polysaccharides based nanofibres are shown to be of great interest to the biomedical research community (Xu, Yang, & Yang, 2009). The high surface area to volume ratio of the polymer nanofibres makes them very suitable for many biomedical applications such as scaffolds used in tissue engineering, drug release, artificial organs, wound healing and vascular grafts (Huang et al., 2011; Bhardwaj & Kundu, 2010). In addition, polysaccharide based hydrogels and microspheres are very promising for protein drug release (Pareta & Edirisinghe, 2006; Elvira, Mano, Roman, & Reis, 2002).

Starch is one of the most abundant naturally occurring polysaccharides with very good biodegradability and bioinertness. In addition, it is a sustainable and renewable biopolymer with excellent biocompatibility. Starch is found as semicrystalline granules of various sizes and shapes in plant tissues, some algae and bacteria. It consists of two homopolymers of D-glucose, amylose and amylopectin. Amylose is a linear polymer with α-D-(1 → 4) glycosidic linkages and amylopectin is a highly branched polymer which consists of α-D-(1 → 6) glycosidic linkages in addition to α-D-(1 → 4) glycosidic linkages at the branching points (Karim, Norziah, & Seow, 2000). However, starch is too brittle to be used on its own and therefore blending it with a polymer in order to form the structures required in novel ways is a hot topic of research (Angellier, Molina-Boisseau, Dole, & Dufresne, 2006; Perez, Perez, Alvarez, & Bernal, 2013; Chivrac, Pollet, Schmutz, & Averous, 2008).

A wide variety of polymeric non-woven fibres from the micro- to nano-scale are usually produced by electrospinning where basically, a nozzle carrying polymeric solution is subjected to high voltage (Edwards, Church, Werkmeister, & Rawshaw, 2009; Welle et al., 2007). The competition between the electric field force and the surface tension force has a significant influence on the fibre forming mechanism. At a critical applied voltage the electric field force can exceed the surface tension force to generate fibres (Zhang & Edirisinghe, 2006; Luo, Stoyanov, Stride, Pelan, & Edirisinghe, 2012). Several biopolymers including starch have been

* Corresponding author. Tel.: +44 2076793920.
E-mail address: suntharavathanan.mahalingam@ucl.ac.uk (S. Mahalingam).

http://dx.doi.org/10.1016/j.carbpol.2014.08.007
0144-8617/

electrospun with excellent surface morphology (Kong & Ziegler, 2013; Matthews, Wnek, Simpson, & Bowlin, 2002; Huang et al., 2013). The electrospinnability of starch depends on the rheological properties and the amount of amylose/amylopectin content in the starch and the ratio of these two ingredients determines the stiffness or flexibility of the fibres (Kong & Ziegler, 2012). However, this method requires high voltage in the kV range and shows poor cost-yield efficiency as a single fibre emerges from the end of the nozzle carrying polymeric solution.

Pressurised gyration is a new technique comprised of simultaneous centrifugal spinning and solution blowing to manipulate the polymeric nanofibre size and their distribution by varying the concentration of the polymeric solution, rotating speed and the working pressure. It is a simple but efficient process allowing the formation of a multitude of parallel polymer nanofibres with regular morphology (Mahalingam & Edirisinghe, 2013). The scale up of production of nanofibres in larger quantities for various applications is very feasible through this technique. This technique makes use of the destabilising centrifugal force and the dynamic fluid flow against the stabilising surface tension of the liquid to fabricate non-woven polymeric nanofibres at very high speed. Unlike electrospinning it is independent of solution properties such as electrical conductivity and dielectric constant. Initially a jet emerges from the orifices in the face of spinneret. This jet further stretches due to centrifugal force and pressure difference at the orifice. Finally, the evaporation of the solvent leads to thinning of the fibres formed.

In this paper, we report on spinnability of starch and starch-loaded polymeric nanofibres using pressurised gyration. In order to improve the spinnability of the starch, poly(ethylene oxide) which is a synthetic semi-crystalline polymer has been added at different concentrations.

2. Experimental

2.1. Materials and rheology

Starch, derived from potato ($(C_6H_{10}O_5)_n$, average molecular weight $Mw \sim 10^6$ g/mol, amylose:amylopectin 25%:75%) was obtained from Sigma Aldrich, UK and used in this investigation. 1 wt%, 5 wt%, 10 wt%, 15 wt%, 20 wt% and 25 wt% of starch was dissolved in deionised water (laboratory grade) and dimethyl sulfoxide (DMSO, Sigma Aldrich, UK) using a water:DMSO weight ratio of 50:50. These were prepared in an air tight bottle and stirred using a magnetic bar at 80 °C for 60 min. Although starch possesses excellent functionality with a diverse range of applications, the poor mechanical properties of the natural polymer led to the development of starch composites (Pereira et al., 2011). Poly(ethylene oxide) (PEO, molecular weight 200 000 g/mol, Sigma Aldrich, UK) was used as a binding polymer. PEO solutions were prepared in deionised water and DMSO using a weight ratio of 50:50. The weight ratio of PEO to starch was varied from 0 to 50% to prepare the PEO–starch mixtures. All these contained 15 wt% of solids, however, the PEO:starch ratio in these was varied (90:10, 70:30 and 50:50). Therefore, the PEO:starch ratio in these are 13.5 wt% PEO and 1.5 wt% starch (90:10), 11.5 wt% PEO and 4.5 wt% starch (70:30) and 7.5 wt% PEO and 7.5 wt% starch (50:50). These were prepared in an air tight bottle and stirred using a magnetic bar at 80 °C for 60 min.

The concentrations of PEO chosen in this work were based on the viscoelastic nature of the polymer. Generally, a lower concentration promotes bead or droplet formation and a higher concentration results in polymer melts where extrusion of fibres is difficult or promotes thicker fibre formation (Katti, Robinson, Ko, & Laurencin, 2004). The viscosity of the starch solutions and PEO–starch suspensions was measured using a Brookfield viscometer. Viscosity data were collected in the shear rate range from 1.32 to 330 s^{-1} at the ambient temperature (~20 °C).

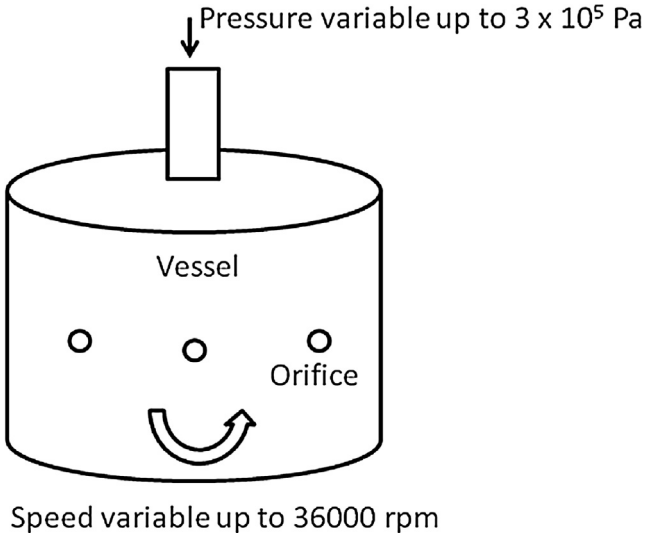

Fig. 1. Schematic diagram illustrating the experimental set-up used for pressurised gyration.

2.2. Pressurised gyration

The experimental set up operating at ambient temperature used in this study is shown in Fig. 1. It consists of a rotary aluminium cylindrical vessel (~ 60 mm in diameter and ~35 mm in height) containing orifices (~20) on its face. The size of one orifice is 0.5 mm. The vessel and orifice dimensions (including the number of orifices) can be varied to suite. One end of the vessel is connected to a motor which can generate speeds up to 36 000 rpm. The other end is connected to a gas stream (e.g. N_2), the pressure of which can be varied up to 3×10^5 Pa. The high speed of the rotating vessel forms a polymer solution jet. This jet subsequently stretches into fibres through an orifice. This stretching can be enhanced by blowing of gas into the vessel. The polymer solution formed in this way undergoes evaporation of the solvent to generate the fibres. To facilitate the collection of polymeric fibres there is a stationary collector made of aluminium foil placed around the spinning vessel.

2.3. Characterisation

The characteristics of the spinning dopes' (whether solution or suspension) and the morphology of fibres formed was studied by optical microscopy (Nikon Eclipse ME600). The latter was also investigated with scanning electron microscopy (SEM, Hitachi S-3400n) at an accelerating voltage of 5 kV. The samples were coated with gold using a sputtering machine (Edwards Sputter S1 50B) for 150 s to minimize charging effects prior to imaging. Statistical analysis on average fibre diameter and diameter distribution of nanofibres was obtained from SEM images. The fibre diameter was calculated using high magnification images with IMAGE J software using ~100 measurements which were made at different locations of the coated samples to calculate the average fibre diameter. For this purpose histograms were made and Gaussian distribution was fitted using Origin software. This was verified by goodness of the fit which was close to 1. The maximum value of the fitted Gaussian distribution curves was noted and taken as the average value. High resolution imaging of the nanofibres was performed using

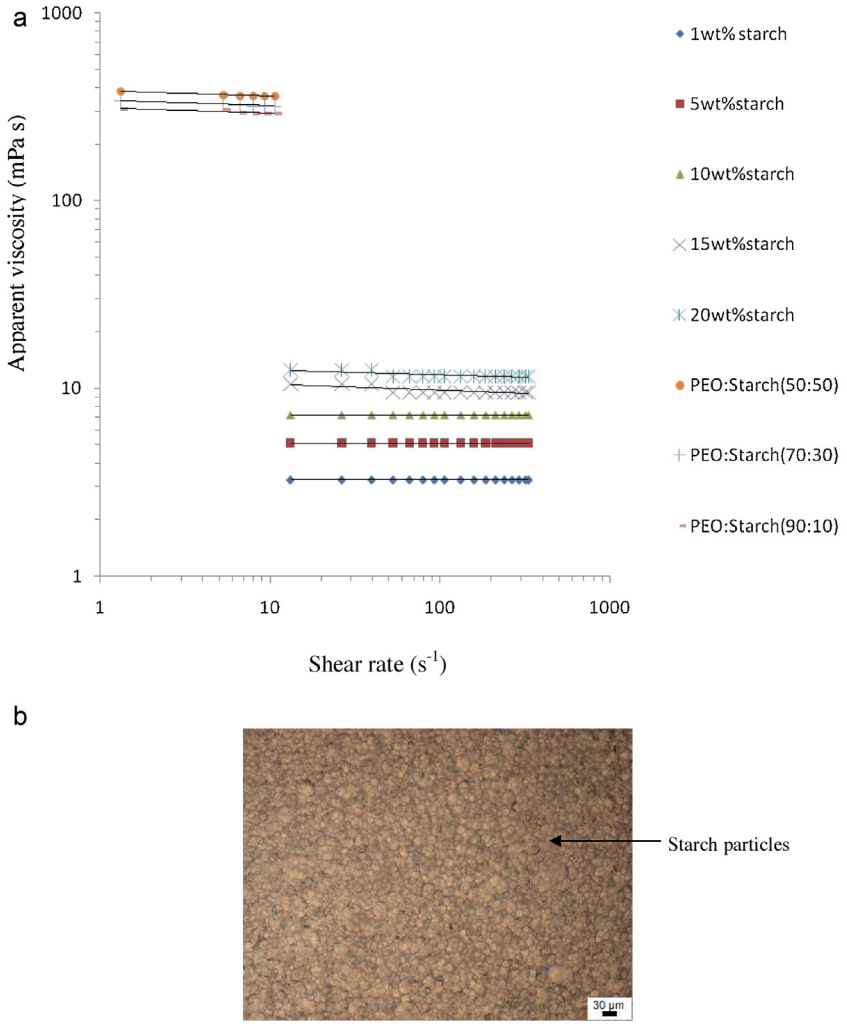

Fig. 2. (a) Flow curves of starch solution and PEO–starch mixtures in DMSO-water at the ambient temperature. (b) Typical optical micrograph of a starch suspension used in this work.

atomic force microscopy (AFM—Bruker) at the ambient temperature. Images were obtained using a tapping mode with a silicon tip having a tip radius of 10 nm. The nominal spring constant of the silicon cantilever is 40 N/m and the scanned rate range was 0.25–0.5 Hz, the resonance frequency used was 276 Hz.

Fourier transform infrared (FTIR) measurements were obtained with a Perkin Elmer 2000 unit in the wave number range 400–4000 cm^{-1} with a resolution of 4 cm^{-1} after accumulation of 30 scans. The spectra were taken in transmission mode for all samples. Background correction for each measurement was done with nitrogen gas.

X-ray diffraction patterns were obtained with a RigaKu D/Max-BR diffractometer operating at 40 kV and 30 mA, over the 2θ range 0–60° with Cu K_α radiation.

Dynamic mechanical thermal analysis (DMTA) of the starch based polymer nanofibrous structures was conducted in tensile mode with a DMA 8000 (Perkin-Elmer) set up (temperature 20 °C and relative humidity 40%). Rectangular samples with a dimension of 4 × 1 mm were made and fitted in the tensile clamps. The measurements were undertaken at a constant frequency of 1 Hz and in a temperature range of 20 °C to 150 °C with a heating rate of 4 °C/min. Prior to measurements load cell calibration was carried out with a known weight and a spring constant. The storage modulus values measured as a function of temperature were smoothened to eliminate noise interference and fitted using Origin software.

3. Results and discussion

3.1. Rheology

Fig. 2(a) shows the flow curves for various concentrations of starch suspensions and PEO–starch mixtures in DMSO/water. In the shear rate range 1.32 s^{-1} to 330 s^{-1} the viscosities of all the suspensions and mixtures prepared were determined except the 25 wt% starch suspension where gelation occurred.

For comparative purposes, the shear viscosities (η_0) were obtained at a shear rate of 1.32 s^{-1} for PEO–starch mixtures. In the case of PEO–starch mixtures, the shear viscosity increased from 291 mPa s to 384 mPa s as the weight percentage of starch increased from 10 to 50. Shear thinning is clearly seen in all the PEO–starch mixtures. Power law fitting $\left(\eta = K\gamma^{n-1}\right)$ for the 50:50 PEO–starch mixture gives $y = 386x^{-0.03}$ (R^2 value of 0.96). Here n is 0.97. Similarly, n is 0.968 and 0.967 for the PEO–starch 70:30 and 90:10 mixtures, respectively, indicating a slightly weaker shear thinning effect. All of the starch suspensions showed Newtonian behaviour over the shear rate range investigated. For starch

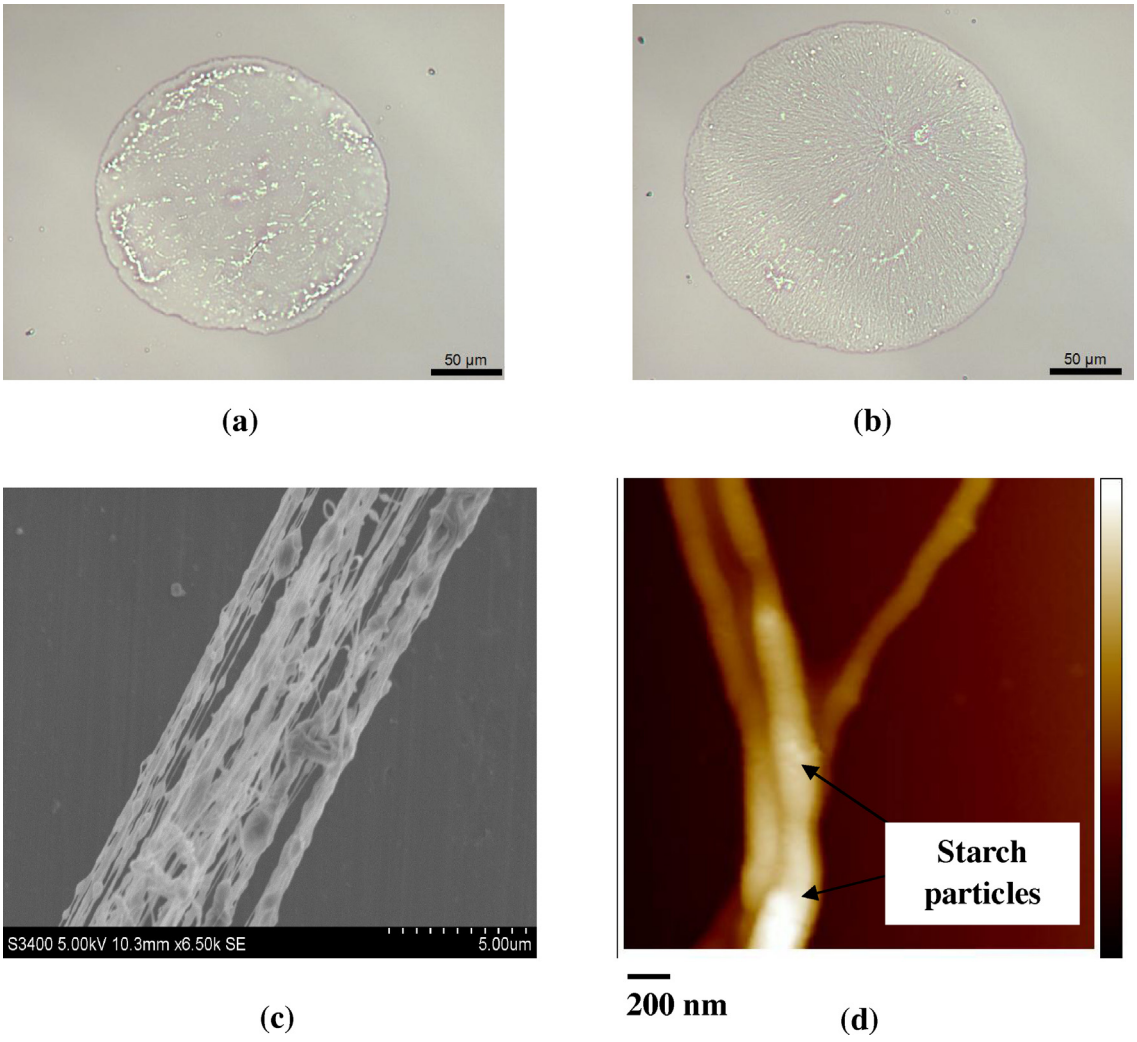

Fig. 3. (a) and (b) Optical micrographs showing starch beads obtained at a rotational speed of 36 000 rpm and a working pressure of 1×10^5 Pa for 1 wt% and 20 wt% of starch, respectively, (c) continuous beaded fibres obtained at a rotational speed of 36 000 rpm and a working pressure of 1×10^5 Pa for 15 wt% starch-loaded PEO (d) AFM image of the nanofibres showing starch in the PEO (see arrow).

suspensions the mean shear viscosity increased from 3.25 mPa s to 11.78 mPa s as the concentration of the starch increased from 1 wt% to 20 wt%.

3.2. Fibre formation

Various concentrations of starch suspensions were used in the pressurised gyration process. They were spun at fixed working pressure with different rotational speeds. Previous work has shown that the formation of fibres and the resulting fibre diameter is greatly influenced by the entanglements in the spinning dope (helped by polymer concentration and its molecular weight) and rotating speed of the pressurised gyration process (Mahalingam & Edirisinghe, 2013). Fig. 3(a) and (b) shows the optical micrographs of the beads obtained in the case of 1 wt% and 20 wt% of starch suspensions spun at 36 000 rpm and a working pressure of 1×10^5 Pa. Fig. 3(c) shows the scanning electron micrograph of the fibres formed from the PEO–starch mixture. In this case, beaded uniform fibres were observed in a well aligned direction. The AFM observations further verify the surface morphology of starch loaded nanofibres as shown in Fig. 3(d). The image clearly shows the nanostructure of the individual fibres formed on a flat surface. It is well known that sufficient polymer entanglement requires a minimum molecular weight or that the entanglement density increases with concentration of the polymer for a given molecular weight (Shenoy, Bates, Frisch, Pelan, & Wnek, 2005). Thus, as the polymer concentration increases, the overlapping of polymer chains form sufficient entanglement networks of polymer chains and higher concentrations of starch only polymer beads were obtained indicating there is no polymer chain entanglement as a result of suspension formation. Thus, sufficient polymer chain entanglement is a prerequisite to form continuous fibres in the pressurised gyration process. It is generally accepted that polymer molecular weight and polymer chain entanglement significantly affect the fibre morphologies (Luo, Stride, Stoyanov, Pelan, & Edirisinghe, 2011). Bead-free continuous fibres are formed when the polymer concentration is above the critical concentration. However, increasing the concentration of the polymer increases the viscosity of polymer solution hindering solvent evaporation and this results in thicker fibres or solidification takes place during spinning and the fibres cannot be formed.

3.3. Starch-loaded PEO nanofibres

Fig. 4 shows the plot of fibre diameter against the rotating speed for PEO–starch mixtures. For comparative purposes the fibres formed from PEO solution is also shown here. A reduction in fibre diameter was observed when increasing the rotating speed up to 36 000 rpm. No fibres were formed at rotating speeds up to

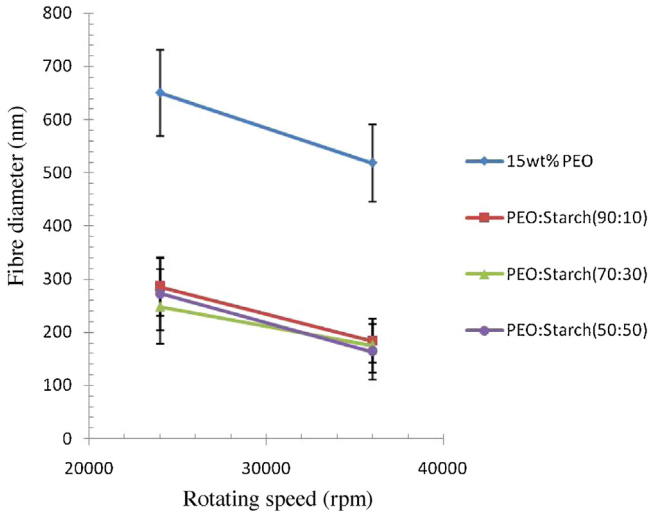

Fig. 4. Plot of fibre diameter variation against the rotating speed for 15 wt% PEO and 15 wt% PEO–starch with different weight ratios of PEO and starch contents at a fixed working pressure of 1×10^5 Pa.

24 000 rpm for PEO polymer solution and PEO–starch mixtures. Only beads were produced at these rotating speeds. For 15 wt% PEO, the fibre diameter is 650 nm at a rotating speed of 24 000 rpm and a working pressure of 1×10^5 Pa. At a similar working pressure and a rotating speed of 36 000 rpm the obtained fibre diameter is 518 nm. For PEO–starch mixture with PEO:starch weight ratio of 90:10, 70:30 and 50:50, the measured fibre diameters were 285 nm, 248 nm and 272 nm, respectively, at a rotating speed of 24 000 rpm. However, at a rotating speed of 36 000 rpm the measured fibre diameters were 184 nm, 175 nm and 163 nm. This shows that there is a minimum rotating speed of 24 000 rpm needed to form fibres. The working pressure had a significant influence on the fibre formability in this process. At a fixed rotating speed, increasing the working pressure above 1×10^5 Pa resulted in rapid evaporation of the solvent and solidification of the spinning dope in the rotating vessel.

Fundamental governing forces in the pressurised gyration process are centrifugal force and forces due to dynamic fluid flow. These coupled forces act against the surface tension of the polymeric solution and are responsible for fibre formation in this process. The centrifugal force accelerates the liquid stream where solvent evaporation and polymer chain elongation occurs

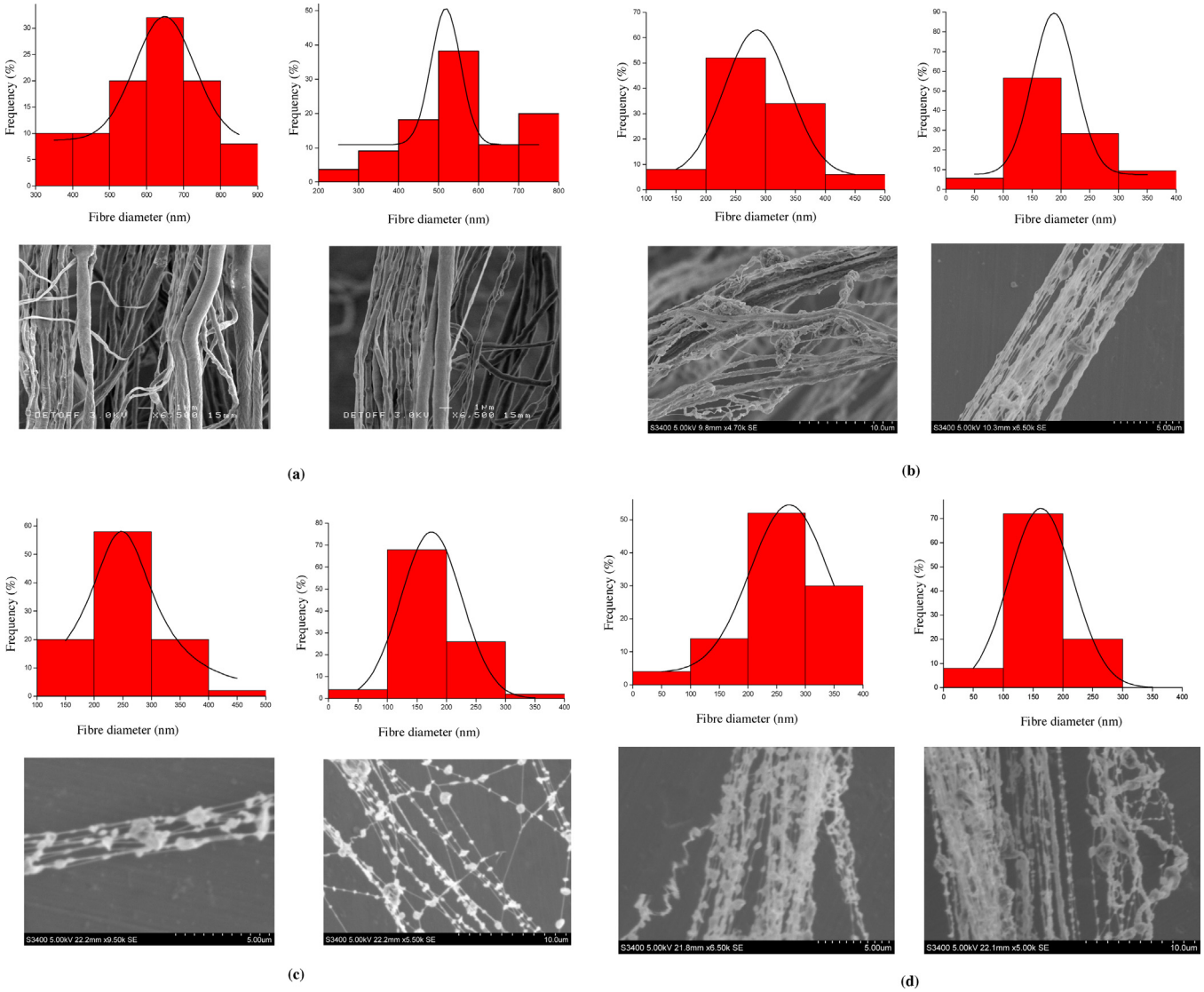

Fig. 5. Diameter distribution and scanning electron micrograph of each starch-loaded PEO system at low (24 000 rpm, left-hand side) and high (36 000 rpm, right-hand side) rotating speeds: (a) PEO only, (b) 90:10 PEO–starch, (c) 70:30 PEO–starch, (d) 50:50 PEO–starch.

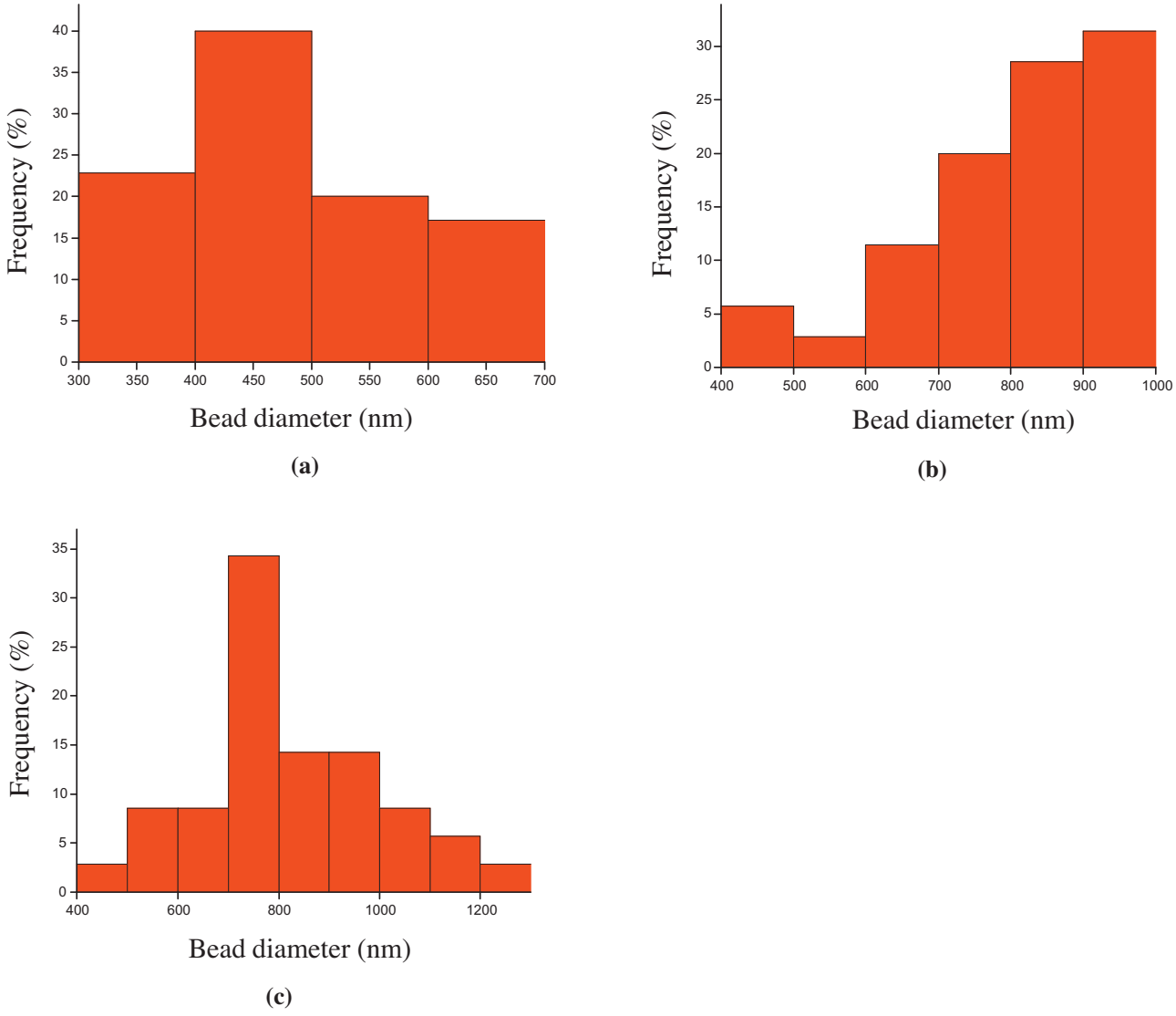

Fig. 6. Distribution of bead diameter in different PEO–starch nanofibres with PEO:starch ratio (a) 90:10 (b) 70:30 (c) 50:50.

(Badrossamay, McIlwee, Goss, & Parker, 2010). This acceleration is enhanced by the gas blowing operation where liquid exerts more force to overcome the surface tension force. The increase of rotational speed during spinning will increase the centrifugal force. This in turn reduces the time constant of forces acting on the polymer solution. The smaller the time constant the more elastic is the response of the polymer chains. Conversely, higher the time constant the viscous response of the polymer increases and therefore there is a need to have a minimum rotational speed to increase the viscous response of the polymer solution for forming fibres from the low concentration of polymer solution (Mahalingam & Edirisinghe, 2013). This is the reason for forming beads in the 15 wt% PEO–starch mixtures and 15 wt% PEO solution at low rotational speed.

Fig. 5(a)–(d) shows the fibre diameter distribution for different processing conditions. It is clearly seen that at 15 wt% of PEO a wider size distribution of fibres is obtained at a lower rotating speed. Increasing the rotating speed produces a narrow size distribution of fibres. However, polydispersity index (standard deviation/mean) of the distribution for these two cases is 12% and 14%, respectively, at a working pressure of 1×10^5 Pa. At a similar working pressure the polydispersity index is 19% and 22% for 15 wt% PEO–starch mixture with a PEO:starch weight ratio of 90:10 at rotating speeds of 24 000 rpm and 36 000 rpm, respectively. When increasing the PEO:starch weight ratio a polydispersity index of 25% and 32% was obtained. This observation shows that the formed fibre diameter and distribution could be controlled through this forming technique. In all cases well aligned fibres were produced. However, beaded fibres were formed due to agglomeration of starch particles in PEO–starch mixture. A distinct advantage of this technique compared to electrospinning is a significant reduction in the random orientation of fibres formed. This is largely due to nonexistence of whipping or non-axisymmetric instabilities and in the absence of an electric field the nonexistence of repulsive forces brought about by surface charges can help to form well-ordered nanofibres (Ajao et al., 2010).

Moreover, in non-Newtonian liquids the existence of normal stresses in contrast to shear stresses represents stresses in the same direction as the deformation plane. This facilitates more stretching of the polymer drawn from the orifice (Gupta & Kothari, 1997). Although the pressurised gyration process takes place at the ambient temperature, the temperature of the jet changes as the solvent evaporates. There is a temperature gradient arising through the jet at a given time. Even at ambient temperature, a higher rotational speed facilitates solvent evaporation through frictional and heat loss which inevitably affects the elongational viscosity. The change

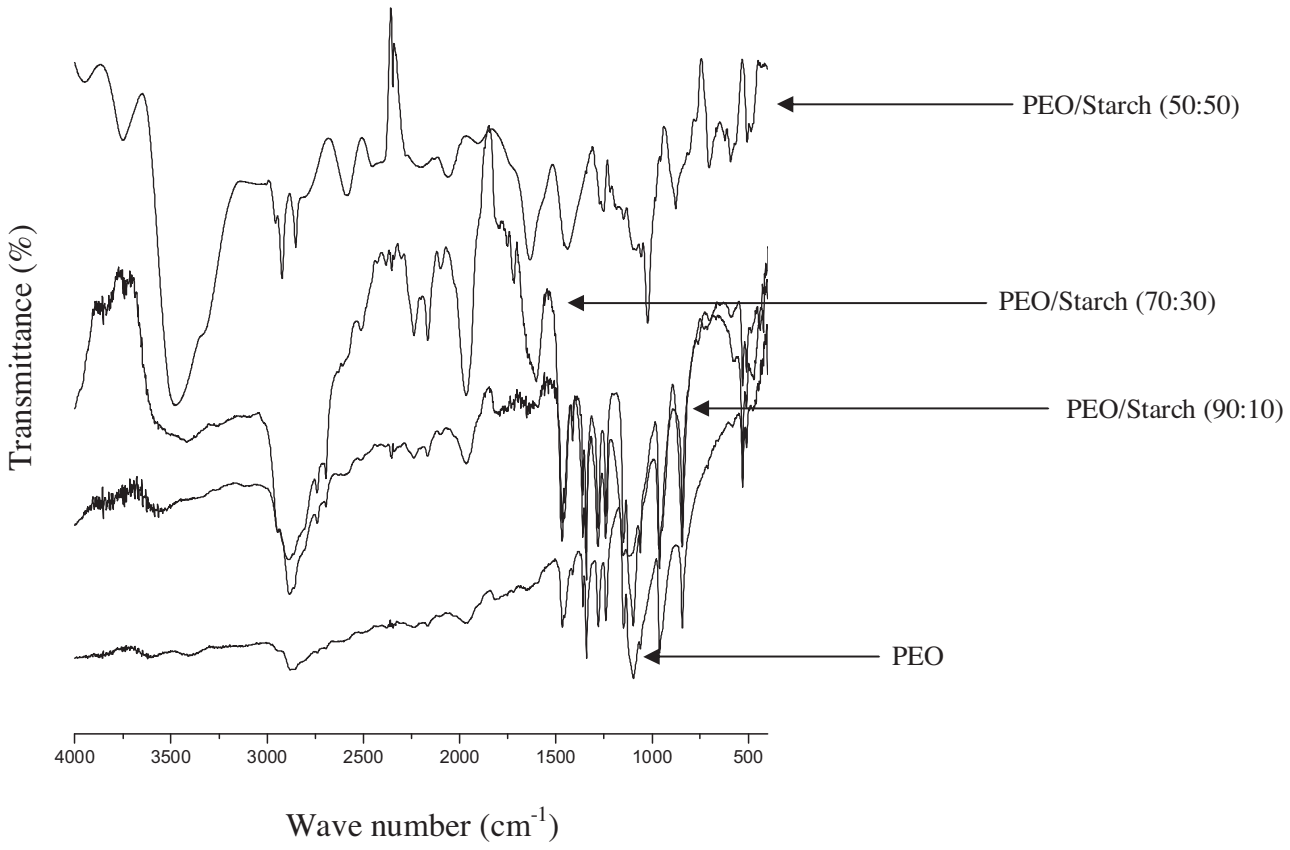

Fig. 7. FTIR traces of various starch-loaded PEO systems.

in elongational viscosity during spinning determines the final fibre diameter and the distribution (Mahalingam & Edirisinghe, 2013).

The formation of beads and beaded fibres is promoted by higher surface tension (Fong, Chun, & Reneker, 1999). The competing action between the surface tension and the viscoelastic forces determine the formation of the smooth fibres. Fig. 6(a)–(c) shows the bead diameter analysis of the formed fibres for various PEO–starch mixtures. The maximum bead diameter obtained when PEO–starch was 90:10 was 700 nm, for 70:30 was 1000 nm and for 50:50 was 1300 nm. This clearly shows that the increase in viscosity increases the bead diameter of the formed fibres. The jet ejected from the orifice shrinks over time and assisted by surface

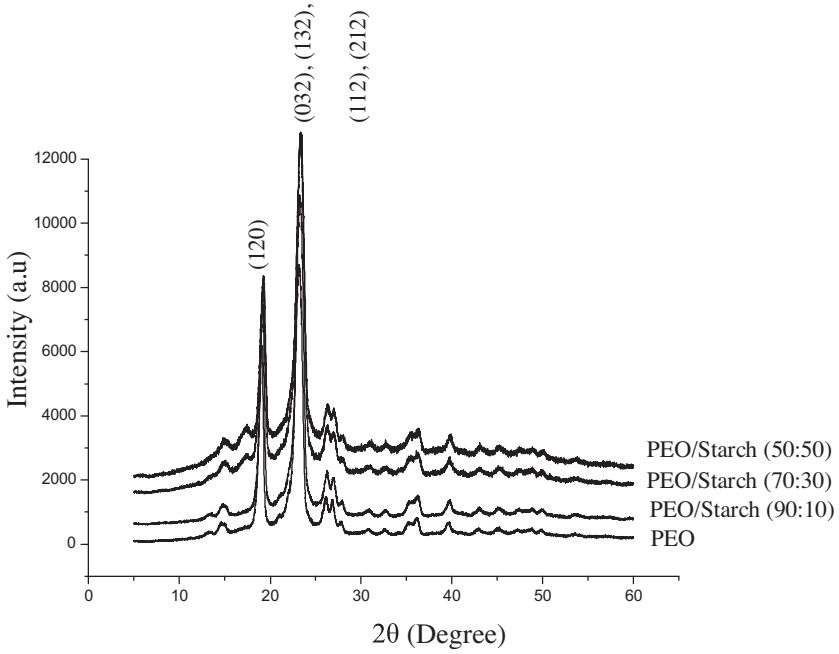

Fig. 8. XRD patterns of various starch-loaded PEO systems. Arbitrary units are indicated by a.u.

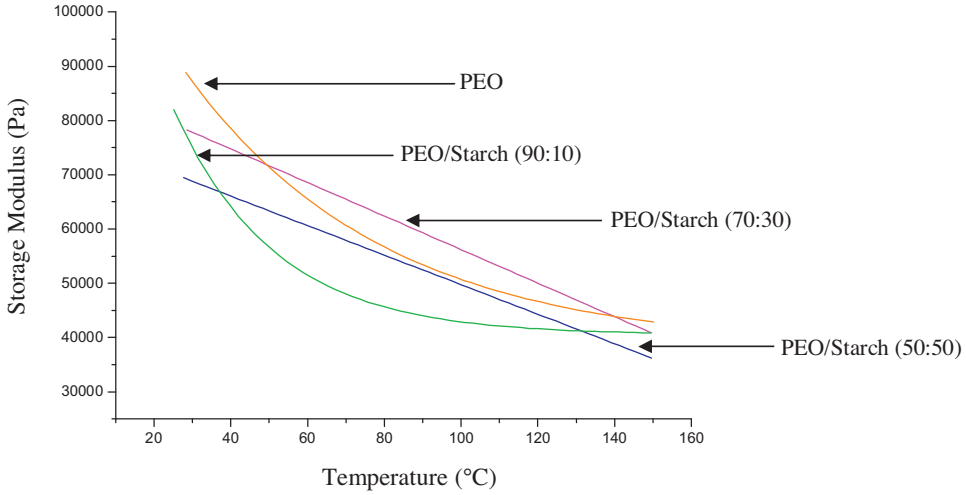

Fig. 9. Storage modulus of different starch-loaded nanofibre products at different temperatures.

tension forms beads. On the other hand, the viscoelastic forces prevent the change in shape due to coiled macromolecules that have a well oriented and entangled network and results in beaded fibres.

Fig. 7 presents the FTIR spectra of the PEO and the PEO–starch nanofibrous structures with varying PEO:starch content. The broad absorption band in the region of wave number 3700–3500 cm^{-1} represents the O—H stretching vibration (Nakason, Wohmang, Kaesaman, & Kiatkamjornwong, 2010). The intensity of the peak increases with the starch content in the composite fibres. There is only a small absorption seen in the PEO nanofibrous structures. This is indicating the water absorption of the PEO–starch composite fibres is greater and increased with the starch content. Further, the peak at 2900 cm^{-1} represents the C—H vibration stretching in the PEO and the starch (Nakason et al., 2010). The broader stretching is obtained in PEO–starch at a weight ratio of 70:30. This is related to the band coalescence and could be attributed to the miscibility of composite. The broadness and the peak intensity of PEO–starch with a weight ratio 90:10 is weaker than the previous case, however they are stronger than the PEO itself. Again this is showing the band coalescence and the miscibility in the composite fibres. The PEO/starch with a weight ratio of 50:50 is showing a weaker peak than the other PEO/starch composites. This might be associated with saturation of the starch in the mixture. This is also suggesting that PEO–starch composite fibres with a weight ratio 90:10 and the 70:30 are more chemically homogeneous than those of the weight ratio of 50:50.

The spectra obtained in 1300–1000 cm^{-1} is associated with the C—O—C and C—O—H vibrational modes (Rubens, Snauwaert, Heremans, & Stute, 1999). It can be clearly seen that the band obtained at these wave numbers are different for PEO and starch-loaded PEO. As shown above, the miscibility and homogeneity of the mixture is evident in the PEO–starch fibres with a weight ratio of 70:30 and 90:10 compared to 50:50. In addition to that a broad band at 2000 cm^{-1} is attributed to the asymmetric stretching of the PEO (Pereira et al., 2011). Further, the presence of characteristic peaks of PEO and starch at 845 cm^{-1} and 1643 cm^{-1}, respectively, shows evidence of the blending of starch in PEO. The broadening of 3421 cm^{-1} and the 1642 cm^{-1} can be attributed to the intermolecular hydrogen bonding between PEO and starch which favours the blending (Jagadish & Raj, 1999).

The crystallinity and structural conformity of the nanofibres prepared are identified using XRD. Fig. 8 shows the XRD patterns of the starch based nanofibrous mats for various concentrations of polymer. The presence of well-resolved peaks in the diffraction patterns in the range from $2\theta = 16^\circ$ to 30° is characteristic of the PEO crystalline structures (Pereira et al., 2011). PEO consists of helical crystalline geometry and its structure is composed of C—C—O—C, C—O—C—C and O—C—C—O conformational arrangements. By invoking the Bragg's law, from the strong peaks at 19.2° and 23.3° the corresponding interplanar distance is determined to be 0.46 and 0.38 nm, respectively. The peak $2\theta = 19.2^\circ$ is related to the crystallographic plane (1 2 0) and the peak $2\theta = 23.3^\circ$ is related several planes—(0 3 2), (1 3 2), (1 1 2), (2 1 2), (0 0 4) and (1 2 4) (Pereira et al., 2011). The starch used has not shown any peak in the PEO:starch (90:10) XRD pattern; however, PEO:starch (70:30) and PEO:starch (50:50) show reflection at $2\theta = 17^\circ$ and this corresponds to B-type crystallites in potato starch (Bajer, Kaczmarek, & Bajer, 2013).

Fig. 9 shows the storage modulus curves for the PEO and the PEO–starch mixtures. At 30 °C, the storage modulus is higher for PEO nanofibres compared to PEO–starch nanofibres. Also, the PEO–starch composition with a weight ratio 90:10 shows a higher storage modulus compared to the other PEO–starch compositions in the temperature range 30–40 °C and is slightly higher than 50:50 composition at 130–150 °C. The storage modulus for all nanofibrous structures reduces with the temperature. A sharper initial decrease is observed for the PEO and the PEO–starch mixture with a weight ratio 90:10. For example, a storage modulus of 78 kPa is obtained for PEO at 40 °C which is ~37% larger than the storage modulus observed at 80 °C. Similarly, a storage modulus of 65 kPa is observed for PEO–starch mixture with a weight ratio 90:10 at 40 °C and this is ~41% larger than the storage modulus observed at 80 °C. However, the rate of reduction of starch modulus is less for PEO–starch mixtures with a weight ratio 70:30 and 50:50. This might be due to the restricted motion of polymer matrix chains due to the increased amounts of starch particles.

The mechanical performance of the starch could be increased by addition of polymers in a controlled manner. This is mainly done by engineering the surface chemistry between the polymer and the starch. Chen et al. (2012) showed that by introducing a filler material to the polymer based composites the mechanical properties could be modified. They have shown that a filler material could be a potent coupling agent and greatly enhances the interfacial interactions and mechanical reinforcement. A threefold increase in storage modulus is observed for nanofibre-polymer matrix composites investigated by Ozden, Menceloglu, and Papila (2010). In fact, they have shown that the inherent cross-linked fibre structure and the surface chemistry of the electrospun fibres led to a significant increase in mechanical response of the composites. The unique current observation is that under ambient conditions as the

PEO content was increased in the starch mixtures, the storage modulus was increased. This will enhances usage of the starch-loaded polymer fibrous structures in biomedical applications where PEO gives more mechanical rigidity to the PEO–starch system.

4. Conclusions

This work demonstrated the spinnability of starch and starch-loaded polymer nanofibres and the formation of nanofibrous structures by pressurised gyration. The starch used realised in suspensions and mapping of apparent viscosity against the shear rate showed Newtonian behaviour at 1–20 wt% of starch and non-Newtonian flow in all PEO–starch mixtures with various PEO:starch weight ratios. The spinning dope's rheological properties played a crucial role in fibre formation in the pressurised gyration process. The starch suspensions formed only beads whereas PEO–starch mixtures generated continuous fibres with starch beads. The PEO acted as a thickener and stabiliser to the starch and acted against its sedimentation in the suspensions.

The present study demonstrates the formation of continuous fibres using PEO–starch mixtures in the pressurised gyration process. The produced fibre diameters are shown to be a function of polymer concentration and rotating speed of the processing system. At a lower rotational speed fibres were not obtained, only beads were formed. Fibres in the range of 650 nm to 160 nm were formed at various rotating speeds and a fixed working pressure. At a fixed rotating speed increasing the working pressure promoted rapid evaporation of solvent and solidification of the spinning dope in the rotating vessel. The morphological characterisation showed that uniform beaded fibres could be obtained with starch-loaded PEO mixtures. The bead diameter is shown to be a function of PEO:starch weight ratio.

The FTIR study showed that good blend miscibility in the nanofibrous structures could be obtained in starch-loaded PEO mixtures. The miscibility at 10% and 30% of starch in PEO is better than the 50%. XRD patterns revealed the characteristic crystalline structure for PEO and B-type crystallites of potato starch in higher concentrations of PEO–starch mixtures. The storage modulus of the nanofibrous structures decreased with increasing temperature, at different rates which were dependent on the temperature but more work in this area is needed in order to uncover general trends for these mixtures which can be exploited in technological applications.

Acknowledgements

The authors are grateful for an EPSRC-UCL Knowledge Exchange Programme Award which initiated this work. The assistance of Dr B. Raimi-Abraham in the UCL School of Pharmacy for AFM and XRD analysis of nanofibres is acknowledged. We like to thank Mr Kevin Reeves (Archaeology Department in UCL) for help with electron microscopy.

References

Ajao, J. A., Abiona, A. A., Chigome, S., Fasaki, A. Y., Osinkolu, G. A., & Maaza, M. (2010). Electric-magnetic field-induced aligned electrospun poly(ethylene) oxide (PEO) nanofibres. *Journal of Materials Science*, *45*, 2324–2329.

Angellier, H., Molina-Boisseau, S., Dole, P., & Dufresne, A. (2006). Thermoplastic starch–waxy maize starch nanocrystals nanocomposites. *Biomacromolecules*, *7*, 531–539.

Badrossamay, M. R., McIlwee, H. A., Goss, J. A., & Parker, K. K. (2010). Nanofibre assemble by rotary jet-spinning. *Nano Letters*, *10*, 2257–2261.

Bajer, D., Kaczmarek, H., & Bajer, K. (2013). The structure and properties of different types of starch exposed to UV radiation: A comparative study. *Carbohydrate Polymers*, *98*, 477–482.

Bhardwaj, N., & Kundu, S. C. (2010). Electrospinning: A fascinating fibre fabrication technique. *Biotechnology Advances*, *28*, 325–347.

Chen, L., Chai, S., Liu, K., Ning, N., Gao, J., Liu, Q., Chen, F., & Fu, Q. (2012). Enhanced epoxy/silica composites mechanical properties by introducing grapheme oxide to the interface. *ACS Applied Materials & Interface*, *4*, 4398–4404.

Chivrac, F., Pollet, E., Schmutz, M., & Averous, L. (2008). New approach to elaborate exfoliated starch-based nanocomposites. *Biomacromolecules*, *9*, 896–900.

Edwards, S. L., Church, J. S., Werkmeister, J. A., & Rawshaw, J. A. M. (2009). Tubular micro-scale multiwalled carbon nanotube-based scaffolds for tissue engineering. *Biomaterials*, *30*, 1725–1731.

Elvira, C., Mano, J. F., Roman, J. S., & Reis, R. L. (2002). Starch-based biodegradable hydrogels with potential biomedical applications as drug delivery system. *Biomaterials*, *23*, 1955–1966.

Fong, H., Chun, I., & Reneker, D. H. (1999). Beaded nanofibres formed during electrospinning. *Polymer*, *40*, 4585–4592.

Gupta, V. B., & Kothari, V. K. (1997). *Manufactured fibre technology*. London, UK: Chapman & Hall (Chapters 2–7).

Huang, C., Niu, H., Wu, C., Ke, Q., Mo, X., & Lin, T. (2013). Disc-electrospun cellulose acetate butyrate nanofibres show enhanced cellular growth performances. *Journal of BioMedical Materials Research A*, *101*, 115–122.

Huang, Z., Lee, H., Lee, E., Kang, S., Nam, J., & Lee, M. (2011). Responsive nematic gels from the self-assembly of aqueous nanofibres. *Nature Communications*, *2*, 459.

Jagadish, R. S., & Raj, B. (1999). Properties and sorption studies of polyethylene oxide–starch blended films. *Food Hydrocolloids*, *25*, 1572–1580.

Karim, A. A., Norziah, M. H., & Seow, C. C. (2000). Methods for the study of starch retrogradation. *Food Chemistry*, *71*, 9–36.

Katti, D. S., Robinson, F. K., Ko, F. K., & Laurencin, C. T. (2004). Bioresorbable nanofibre-based system for wound healing and drug delivery: Optimization of fabrication parameters. *Journal of Biomedical Materials Research B—Applied Biomaterials*, *70*, 286–296.

Kong, L., & Ziegler, G. (2012). Role of molecular entanglements in starch fibre formation by electrospinning. *Biomacromolecules*, *13*, 2247–2256.

Kong, L., & Ziegler, G. (2013). Quantitative relationship between electrospinning parameters and starch fiber diameter. *Carbohydrate Polymers*, *92*, 1416–1422.

Luo, C. J., Stoyanov, S. D., Stride, E., Pelan, E., & Edirisinghe, M. J. (2012). Electrospinning versus fibre production methods: From specifics to technological convergence. *Chemical Society Reviews*, *41*, 4708–4735.

Luo, C. J., Stride, E., Stoyanov, S. D., Pelan, E., & Edirisinghe, M. J. (2011). Electrospinning short polymer micro-fibres with average aspect ratios in the range of 10–200. *Journal of Polymer Research*, *18*, 2515–2522.

Mahalingam, S., & Edirisinghe, M. J. (2013). Forming of polymer nanofibres by a pressurised gyration process. *Macromolecular Rapid Communications*, *34*, 1134–1139.

Matthews, J. A., Wnek, G. E., Simpson, D. G., & Bowlin, G. L. (2002). Electrospinning of collagen nanofibres. *Biomacromolecules*, *3*, 232–238.

Nakason, C., Wohmang, T., Kaesaman, A., & Kiatkamjornwong, S. (2010). Preparation of cassava starch-graft-polyacrylamide superabsorbents and associated composites by reactive blending. *Carbohydrate Polymers*, *81*, 348–357.

Ozden, E., Menceloglu, Y. Z., & Papila, M. (2010). Engineering chemistry of electrospun nanofibres and interfaces in nanocomposites for superior mechanical properties. *ACS Applied Materials & Interfaces*, *2*, 1788–1793.

Pareta, R., & Edirisinghe, M. J. (2006). A novel method for the preparation of biodegradable microspheres of protein drug delivery. *Journal of the Royal Society Interface*, *3*, 573–582.

Pereira, A. G. B., Paulino, A. T., Nakamura, C. V., Britta, E. A., Rubira, A. F., & Muniz, E. C. (2011). Effect of starch type on miscibility in poly(ethylene oxide) (PEO)/starch blends and cytotoxicity assays. *Materials Science and Engineering C*, *31*(2), 443–451.

Perez, E., Perez, C. J., Alvarez, V. A., & Bernal, C. (2013). Fracture behaviour of a commercial starch/polycaprolactone blend reinforced with different layered silicates. *Carbohydrate Polymers*, *97*(2), 269–276.

Rubens, P., Snauwaert, J., Heremans, K., & Stute, R. (1999). In situ observation of pressure-induced gelation of starches studied with FTIR in the diamond anvil cell. *Carbohydrate Polymers*, *39*, 231–235.

Shenoy, S. L., Bates, W. D., Frisch, H. L., Pelan, E., & Wnek, G. E. (2005). Role of chain entanglements on fibre formation during electrospinning of polymer solutions: Good solvent, non-specific polymer–polymer interaction limit. *Polymer*, *46*, 3372–3384.

Welle, A., Kroger, M., Doring, M., Niederer, K., Pindel, E., & Chronakis, I. S. (2007). Electrospun aliphatic polycarbonates as tailored tissue scaffold materials. *Biomaterials*, *28*, 2211–2219.

Woodings, K. (2001). *Regenerated cellulose fibres*. Cambridge, UK: CRC Press LLC, Woodhead Publishings Ltd (Chapter 1).

Xu, W., Yang, W., & Yang, Y. (2009). Electrospun starch acetate nanofibres: Development, properties, and potential application in drug delivery. *Biotechnology Progress*, *25*, 1788–1795.

Zhang, H. B., & Edirisinghe, M. J. (2006). Electrospinning zirconia fibre from a suspension. *Journal of the American Ceramic Society*, *89*(6), 1870–1875.